Journal of Applied Electrochemistry (2005) 35:641–653
DOI 10.1007/s10800-005-1628-5

Reviews in Applied Electrochemistry Number 57

Thick titania films for semiconductor photocatalysis

ANDREW MILLS,* GEORGE HILL, MATTHEW CROW and STEPHANIE HODGEN
Department of Pure and Applied Chemistry, University of Strathclyde, Glasgow, G1 1XL, UK
*(*author for correspondence, e-mail: a.mills@strath.ac.uk)*

Received 26 July 2004; accepted in revised form 24 October 2004

Key words: semiconductor, photocatalysis, titania, thick-films, stearic acid, porosity

Abstract

A brief overview of work carried out by this group on thick (>1 μm), optically clear, robust titania films prepared by a sol–gel method, as well as new results regarding these films, are described. Such films are very active as photocatalysts and able to destroy stearic acid with a quantum yield of 0.32%. The activity of such films is largely unaffected by annealing temperatures below 760 °C, but is drastically reduced above this temperature. The drop in photocatalyst activity of such films as a function of annealing temperature appears to correlate well with the change in porosity of the films and suggests that the latter parameter is very important in deciding the overall activity of such films. The importance of porosity in semiconductor photocatalysed cold combustion may be due to the effect it has on access of oxygen to the active sites, rather like the effect the position of a fire grate (open or closed) has on the rate of burning, i.e., hot combustion, that takes place in a fireplace.

1. Introduction

Self-cleaning glass has been hailed as one of the greatest of all inventions [1] and certainly represents the most important advance in glass technology for many decades. A key feature of self-cleaning glass is a thin layer, typically 15 nm thick, of titanium dioxide which is able to absorb some of the UV component of sunlight to drive the photocatalytic mineralisation of many carbon-containing compounds [1–5]. The overall process of semiconductor photomineralisation may be summarised as follows:

$$\text{organic pollutant} + O_2 \xrightarrow[TiO_2]{h\nu \geq E_{bg}} \text{mineralised products} \quad (1)$$

Obviously, with self-cleaning glass the outer titania film must adhere strongly to the glass substrate and be optically clear. Most manufacturers of self-cleaning glass have been able to achieve this using nanocrystalline titania laid down via a chemical vapour deposition method [1, 2, 6]. The titania films must usually be very thin, ca. 15 nm as noted earlier and comprised of nanocrystalline particles, since any thicker, with bigger particles, and the film develops a degree of opacity and/or fragility that renders it unacceptable as a commercial product. Unfortunately titania is an indirect semiconductor and, as a result, although it possesses a bandgap of 3–3.2 eV, it does not absorb strongly in the UVA region (320–380 nm), where most of the UV component of sunlight lies [7]. For example, the absorption coefficient for nanocrstalline anatase, α, is ca. 5×10^4 cm^{-1} at 365 nm [7] and, given for any film:

$$\text{Absorbance} = 0.434\,\alpha\,d(1-p) \quad (2)$$

where p is the porosity and d is the thickness of the film. It follows that a 15 nm, non-porous, titania film, such as Activ^{TM} will only absorb ca. 7% of the incident UVA irradiation at this wavelength [7]. There is interest, therefore, in ways to generate thick films of titania, typically >1 μm, which are optically clear and robust. In a recent series of papers [8–10] this group has reported on a method for producing such films and shown them to be highly active for mediating the photocatalytic destruction of carbon-containing materials, such as stearic acid and soot. This paper highlights the results of this work and also describes more recent work that may help further our understanding of the key factors that decide the overall activity of photocatalytic films.

2. Experimental

2.1. *Materials and methods*

Unless stated otherwise all chemicals were purchased from Aldrich Chemicals (UK) and used as received.

UV/Vis absorption spectra were recorded using a Lambda 20 UV/Vis spectrophotometer (Perkin Elmer, UK).

In the study of the photocatalytic activities of the various titanium dioxide films, stearic acid was used as the test organic material for mineralisation. Stearic acid was chosen as it provides a good representation of the organic solid films that deposit on window glass and because it is very readily deposited to create films that are easily analysed by transmission FT-IR. Each film under test was coated with an initial layer of stearic acid by dropping 0.3 cm^3 of a stearic acid in chloroform solution (30 g dm^{-3}) onto the surface of the film and then spinning it at 500 rpm for 10 s. Each film was then placed in an oven at 100 °C for 30 s and then allowed to cool to room temperature. A 1600 FT-IR (Perkin Elmer, UK) was used to record the FT-IR spectra of the films with an initial stearic acid coating, before and after any illumination. For any and every film, the FT-IR spectrum of the stearic acid coating was used to calculate the integrated area under the stearic acid peaks over the range 2500–3500 cm^{-1}, from which the concentration of stearic acid on the film was calculated as a function of irradiation time, given an integrated absorbance of 1 cm^{-1} is equivalent to 3.13×10^{15} molecules of stearic acid per cm^2 [11]. Through this process, FT-IR absorption spectroscopy allowed the concentration of stearic acid on a test substrate to be measured (in units of molecules of stearic acid cm^{-2}) and monitored as a function of irradiation time.

In the study of the photocatalytic activities of the various films using the stearic acid test system the irradiation source comprised six 8 W black blue fluorescent tubes, set in a half cylinder unit, with a backing aluminum reflector. In all cases the sample under test was placed on the bench and the irradiation unit placed 13 cm above it and facing the film. The light output of this illumination source was determined by ferrioxalate actinometry to be 8.02×10^{17} photons cm^{-2} min^{-1}.

2.2. *Preparation of the thick titanium dioxide films*

The general preparation of thick titanium dioxide films by a sol–gel method is described in detail elsewhere [9]. Briefly 4.65 g of acetic acid was added to 20 ml of titanium isopropoxide under an inert nitrogen atmosphere. To this was added 120 ml of 0.1 mol dm^{-3} nitric acid and, after mixing, the reaction solution was heated rapidly to 80 °C whereupon it turned milky white and opaque. Within a few minutes at this temperature the reaction solution gelled but became fluid again within 1–2 h. The reaction solution was maintained at 80 °C for 8 h whereupon it was allowed to cool to room temperature and any remaining aggregate particles were removed using a 0.45 μm syringe filter. 80 ml of the colloidal solution product were then placed in a Teflon pot with a lid in an autoclave (Parr Instruments, UK) and heated and maintained at 220 °C for 12 h. This hydrothermal step was used to grow the titania particles from ca. 5 to 15 nm. Upon removal of the solution from the autoclave the separated out colloidal particles were redispersed using ultrasound. The reaction solution was then concentrated to about 12 wt% using a rotary evaporator, followed by the addition of 50 wt% Carbowax 20M to help prevent the formation of small surface cracks that are often produced when the paste is cast and allowed to dry.

The final form of the titanium dioxide paste is a white, mayonnaise-like, substance which is stable for many months if kept in the fridge. Unless stated otherwise, all titanium dioxide films produced in this work were generated from the white titanium dioxide paste and so are referred to as 'TiO_2 paste films.' It is assumed that the white colour of the TiO_2 white paste is due to light-scattering by loosely bound, large aggregates of the electrostatically stabilised, small (10–15 nm) colloidal particles of titania. Work carried out by Zaban and his co-workers on a similar system indicates that such aggregated particles may be as large as 3 μm [12]. A striking feature of this paste is that, although initially white when wet, when cast as a film it dries to produce a clear film. The paste can be cast to produce thick ($>>1\mu$m) films using a doctor-blade technique, in which a small amount of the paste is placed on a standard glass microscope slide, between two tracks of Scotch Magic Tape^{TM}, typically ca. 1 cm apart, and subsequently smeared along the gap between the tracks by a flat blade, to produce a final long strip of the TiO_2 paste film on the slide.

Figure 1 illustrates the typical variation in the absorption spectrum of the titania paste film produced by this doctor blade method as it dries and clarifies. The thickness of the film, typically 60 μm when wet, decreases as the film dries and eventually approaches a value of 4–5 μm. How and why the loosely held networks of large aggregates of nanocrystalline titania particles that form the white paste produce a final film that is devoid of such large, light-scattering, aggregates during the drying/clarification process, is not obvious and requires further investigation. However, that the final product is optically clear, i.e. non-scattering and strongly UVA-absorbing is illustrated by the UV/Visible absorption spectrum of the final, dried film in Figure 1.

Although the final stage of the titania film synthesis involved placing the freshly dried film directly into a furnace set at 450 °C for 30 min, no change in the optical characteristics of the 4–5 μm titania films were observed as a result of this treatment. Instead, this final high temperature treatment appears simply to fuse the nanocrystalline titania particles together, burn off any organic present and help bind the titania to the glass to produce a more robust film. Further work shows that even without this heat-treatment step the titania photocatalyst film is very active. X-ray analysis of the titanium dioxide films showed the films before and after the final annealing step to be anatase and SEM analysis showed that the final films comprised particles typically

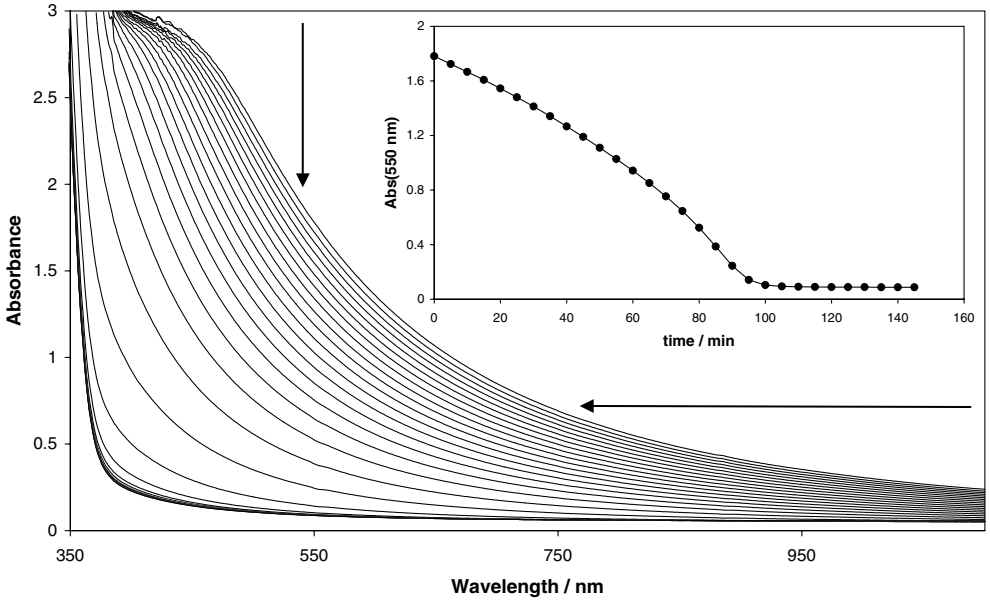

Fig. 1. UV/Vis absorption spectra of a thick paste TiO_2 freshly cast film as it dries in air under ambient conditions. The absorption spectra were recorded every 5 min and the absorbance of the film decreased with increasing drying time. This feature is highlighted in the insert diagram, a plot of the absorbance of the film at 550 nm as a function of drying time, with the data taken from the main diagram.

13 ± 1 nm in diameter. Work by others showed that such films were largely mesoporous with an average porosity of ca. 50–60%.

X-ray powder diffraction patterns for the different titania films were recorded using a Siemens D500 powder diffractometer, fitted with a Kristalloflex 710 generator with a tube head mounted at an angle of 30° from the vertical and operated at 40 kV and 20 mA. The target material was copper producing X-rays of 1.5406 Å. The post-sample radiation was detected by a scintillation counter, after first passing through a post-sample monochromator. Samples were scanned over a range of 2θ values from 20° to 80° using a step scan mode (0.05 degrees step size and 2 s count time per step). Intensity readings were recorded as a function of 2θ°.

AFM images of the films were recorded in air using a Digital Instruments Nanoscope Multimode SPM with a JV-type scanner and a Nanoscope III controller. Olympus tapping mode, silicon pyramidal, cantilevers were used, with a tip curvature <10 nm and a normal force constant of 42 N/m. For all samples both amplitude and height scans were carried out with scan sizes from 1 to 5 μm, recorded at a scan rate of 0.5–1.0 Hz and with a resolution of 512 scan lines per image. No image processing was carried out on the presented data.

3. Results and discussion

3.1. *Photocatalytic activity studies*

The rate of the photocatalytic destruction of stearic acid ($CH_3(CH_2)_{16}CO_2H$) is commonly used to provide a measure of the photocatalytic activity of any new material [11, 13–15]. The overall process may be summarised as follows:

$$CH_3(CH_2)_{16}CO_2H + 26O_2 \xrightarrow[\text{Semiconductor}]{h\nu \geq \text{band gap energy}} 18CO_2 + 18H_2O \quad (3)$$

Since the process involves the transfer of 104 electrons, it follows that the quantum yield for this process will be, at best, ca. 0.01, and this fact should be borne in mind when the measured quantum yields for Reaction (3) are considered later in this article. Since the melting point of stearic acid is markedly above room temperature, i.e. 69.3 °C, it forms solid films when deposited, usually by a spin- or dip-coating technique, on the substrate under test. As noted earlier, the destruction of stearic acid is readily monitored by FT-IR absorbance spectroscopy, since this compound has a peak at 2957.5 cm^{-1}, due to the asymmetric in-plane C–H stretching mode of the CH_3 group, and peaks at 2922.8 and 2853.4 cm^{-1}, due to the asymmetric and symmetric C–H stretching modes of the CH_2 group, respectively.

The FT-IR method employed in this work actually measures the kinetics of the disappearance of stearic acid and here and elsewhere it is assumed that this is also a direct measure of the kinetics of Reaction (3), the photocatalytic destruction of stearic acid, as would be the case if no major long-lived intermediates were generated. Support for this assumption is provided by the work of others [13–15] that shows: (a) the removal of stearic acid by semiconductor photocatalysis produces no film component other than stearic acid that is detectable by FT-IR, (b) no gas phase products other than carbon

dioxide and water are generated during the course of the photocatalytic reaction and (c) the calculated ratio of the number of moles lost due to the disappearance of stearic acid and the concomitant appearance of carbon dioxide is 1:18, as expected for the photocatalytic mineralisation of stearic acid, described by Reaction (3).

Figure 2 illustrates the observed variation in the FT-IR absorbance spectrum of a typical stearic acid film, deposited on a thick (4.5 μm) paste TiO_2 film on a glass slide, as a function of irradiation time with UVA light (365 $\pm$ 25 nm) from the six 8 W BLB illumination system. From the data in Figure 2 it is clear that the stearic acid FT-IR peaks disappear with ultra-band gap irradiation of a TiO_2 paste film, as expected from Reaction (3). Using the data illustrated in Figure 2, the integrated areas under the absorption peaks, due to stearic acid, as a function of irradiation time were calculated and plotted to generate an integrated absorbance versus irradiation time decay profile. The results of this work are illustrated in Figure 3, along with the decay profile, calculated in a similar fashion, for a stearic acid film on plain glass. Stearic acid does not absorb UVA light, thus it is no real surprise that, in the absence of titania film coating, it does not undergo any appreciable decomposition upon illumination with UVA light, as illustrated by the results in Figure 3 for plain glass. In contrast, the FT-IR absorbance versus time profiles recorded for the thick paste TiO_2 film irradiated with 365 nm light, also illustrated in Figure 3, show that under the experimental conditions employed the film is able to photocatalyse the complete destruction of stearic acid within ca. 50 min.

3.2. *Kinetics of photocatalysis*

The kinetics of the photocatalytic destruction of stearic acid, via Reaction (3), were studied as a function of initial stearic acid concentration, over the range: $(1.2–5.6) \times 10^{16}$ molecules of stearic acid cm^{-2}, i.e. 64–300 nm thick. Some of the stearic acid concentration versus irradiation time decay profiles did show some evidence of a tail to the decay profiles, particularly at high stearic acid levels, as illustrated in Figure 3. This latter feature has been suggested by others to be due to the accumulation of a small amount of material that is more difficult to destroy [14]. However, for the most part, the rate of decay appeared largely independent of the stearic acid concentration as illustrated by the results in Figure 4, and the subsequent plot of the initial rate data versus stearic acid concentration, illustrated in the insert diagram of Figure 4. Such zero-order kinetics for Reaction (3) have been reported by others [14, 15] in similar studies and are usually attributed to the complete coverage of the titania photocatalyic active sites by the stearic acid. This appears a likely situation in this work given that the initial stearic acid concentrations employed corresponded to films 25–120 monolayers thick [8].

The FT-IR absorbance versus time decay profiles, as illustrated in Figure 3, were determined for a commercial, self-cleaning, titania film (Activ^{TM}) as well as a thick titania film. For each recorded profile it was possible to determine the initial rate of destruction of stearic acid as a function of time for the film under test, first in units of integrated absorbance (i.e. peak area)/min (simply the gradient of the initial part of the decay

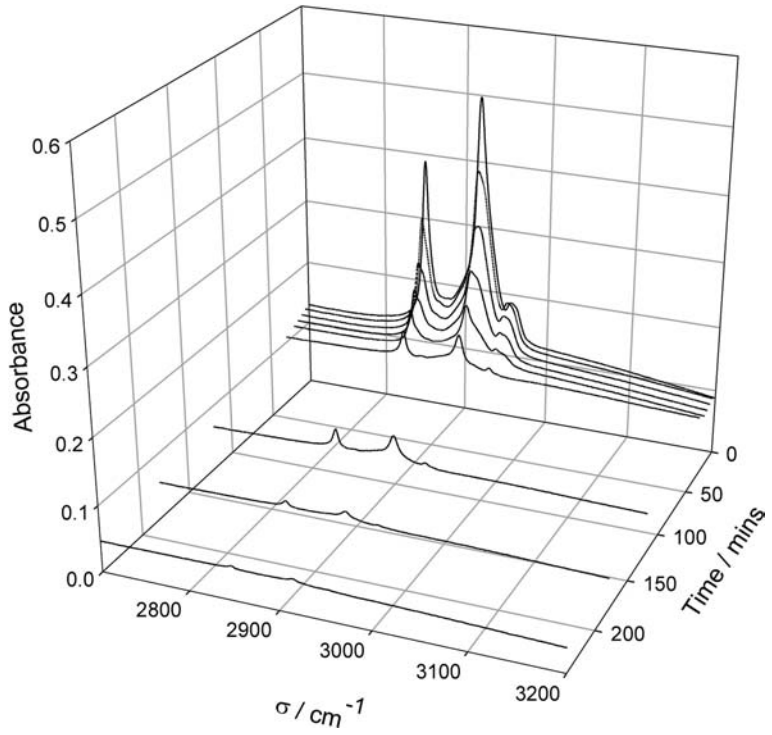

Fig. 2. Recorded decrease in the FT-IR absorbance spectrum of a stearic acid film on a typical, 4.5 μm thick paste TiO_2 film as a function of irradiation time.

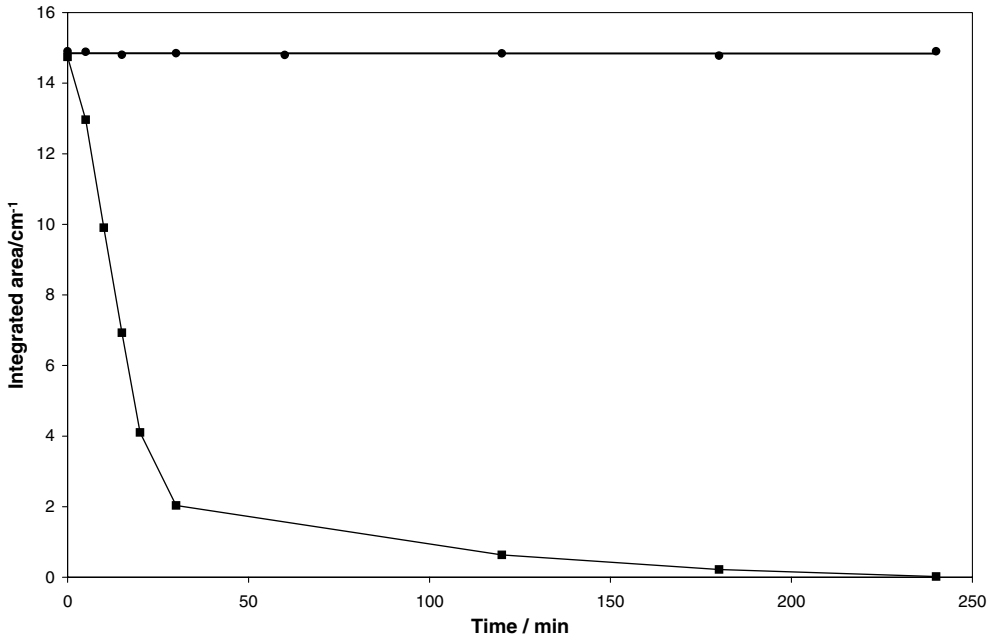

Fig. 3. Plot of the integrated area under the FT-IR absorbance spectrum of a stearic acid layer on: a typical thick TiO_2 paste film (■) and on plain glass (●), as a function of irradiation time.

curves in Figure 3) and then, as the more useful parameter, R_i, (units: molecules of stearic acid/cm^2/min). The calculated initial rates for Reaction (3), in these latter units, for a typical thick paste and Activ^{TM} titania film are listed in Table 1. For each sample, the incident light intensity, I_o, and the fraction of UV light absorbed by the film f, are known or readily calculated, thus it was possible to calculate the quantum yield for each film tested for the overall photomineralisation process, Reaction (3), ϕ, where

$$\phi = \frac{\text{initial rate of disappearance of stearic acid}(R_i)}{\text{rate of light absorption}(= I_o \times f \times (1 - R_{refl}))} \quad (4)$$

where, R_{refl} is the fraction of light reflected by the film. For smooth films of anatase (refractive index = 2.5), such as the Activ^{TM} and paste films, a value of 0.18 can be estimated for R_{refl}. The results of the quantum yield calculations for the Activ^{TM} and paste films are given in

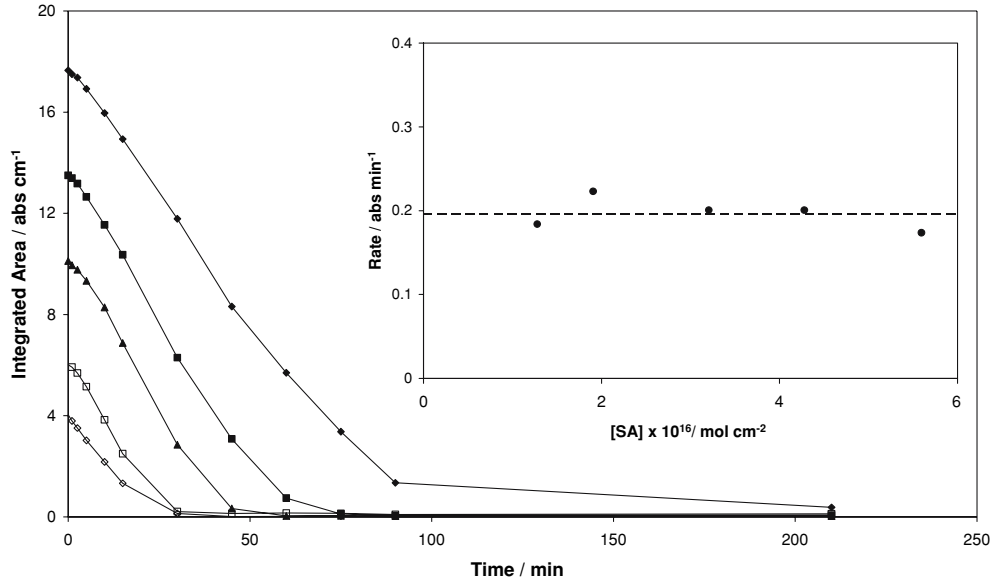

Fig. 4. Plot of a series of profiles of the form: integrated area under the stearic acid peaks, as measured by FT-IR, as a function of irradiation time. Each profile corresponds to a different initial amount of stearic acid, but the same thick TiO_2 paste film was used throughout. The insert diagram is a plot of the initial rate (taken from the data in the main diagram) as a function of initial stearic acid concentration, as determined from the measured initial integrated area [8].

Table 1. Optical and photocatalytic properties of titania-coated glass samples

Film type	Film thickness (d) /nm	Initial rate (R_i)/(10^{13} molecules/cm^2/min)	Fraction of light absorbed (f)[a]	Quantum yield[b] /(10^{-2})
Paste (thick)	4500	144.0	0.70	0.32
Activ^{TM}	15	0.6	0.07	0.01
P25	1300	–	1[c]	0.15[c]

[a]f, calculated using $f = (1 - 10^{-Abs(\lambda)})$ for Activ^{TM}, with absorbance calculated using the formula: $Abs_\lambda = 0.434\alpha_\lambda d(1-p)$, where $\alpha_{365} = 5\times10^4$ cm^{-1} [7] and $p = 0$; for the Paste(thick) films f was calculated from an analysis of the overlap of the UV/Vis spectra of the film with that of the emission spectrum of the lamp.

[b]Quantum yield, ϕ, calculated as: $\phi =$ initial rate/($f \times I_o$ (1-R_{refl})); where $I_0 = 8.02 \times 10^{17}$ photons cm^{-2} min^{-1} and $R_{refl} = (2.5-1)^2/(2.5+1)^2 = 0.18$.

[c]Actually the formal quantum efficiency (FQE), δ, for this material reported by others [11], given it has had to be assumed $f = 1$ and $R_{refl} = 0$ and, by definition, δ = rate of stearic acid destruction (molecules removed/cm^2/min)/incident light intensity (photons/cm^2/min).

Table 1, along with those, reported by others, for a 1.3 μm film of the ubiquitous titania pigment, Degussa P25 [11]; a material which is noted for its high photocatalyst activity and commonly employed as a reference photocatalyst material. The quantum yield data in Table 1 for the thick paste, and P25 films are not highly dissimilar, i.e 0.32 and 0.15, respectively, with the thick paste TiO_2 film appearing somewhat more active than the P25 film. However, the apparent enhanced photocatalytic activity of the thick paste titania film over one of P25 is likely to be fortuitous, since the latter films are white, opaque and scattering and so values for f and R_{refl} cannot be easily determined. Instead, the values for f and R_{refl} for this latter film are assumed to be unity and zero, respectively and, thus the reported quantum yield for this film should be more accurately referred to as a measure of its formal quantum efficiency, the value of which is likely to be a lower estimate of the film's true quantum yield [3]. The results in Table 1 are encouraging in that the subject of this work, namely: thick paste films, appear at least to be on a par with P25 titania, a material which is recognized as being one of the most active commercial forms of titania.

The major problem with films of Degussa P25 TiO_2 is their lack of mechanical stability, since they can be readily wiped off and are easily damaged. In contrast, thick sol–gel films are mechanically robust, undamaged, when wiped, and are not removed by successive applications and removals of Scotch Tape^{TM}; the so-called 'Scotch Tape^{TM} test'. Note that since the maximum quantum yield for this process is likely to be ca. 1%, the calculated quantum efficiency of the thick paste film of 0.32% is very high and indicates that the material is very efficient for promoting the photocatalytic Reaction (3).

In contrast to thick paste and P25 titania films, Activ^{TM} appears to comprise particles that are relatively inactive in terms of photocatalytic activity. Thus, the quantum yield for Reaction (3) was estimated as 0.01%, for Activ^{TM}, ca. 32 times lower than that for a typical thick paste film. It could be that, for reasons not clear at present, the titania produced by a CVD process is inherently less active than that produced using a sol–gel thick paste or flame-hydrolysis (P25) route. However, another suggestion is that photocatalytic activity may be related to film porosity, since both the sol–gel and the P25 films are very porous (% porosity > 50%), whereas, from SEM and AFM images, the Activ^{TM} film is comprised of particles which are very closely packed, producing largely non-mesoporous films [6, 8]. Additional evidence that film porosity may play an important role in deciding the activity of a semiconductor photocatalyst is provided later on in this paper.

3.3. *Photocatalyst durability*

An important characteristic of any photocatalyst is durability. Certainly, many semiconductors appear, on paper at least, to be a much better choice as a photocatalyst than titania, especially if the overall goal is to utilise sunlight to drive the photocatalytic process forward. However, almost all fail to deliver, usually on the grounds of poor durability. Few semiconducting materials can match titania's chemical and biological inertness, high photocatalytic activity and excellent resistance to photochemical ageing. Figure 5 illustrates the observed variation in integrated area due to stearic acid on a thick paste TiO_2 film as a function of irradiation time in an experiment which involved the repeated deposition of stearic acid on the same titania paste film and its subsequent irradiation [8]. The results in Figure 5 indicate that the photoactivity of a thick paste titania film does not diminish with repeated irradiation and help reinforce the reputation of this photocatalyst material for high photochemical durability. In contrast, most other semiconducting materials, especially those with bandgaps that fall into the visible region, either exhibit little or no photocatalytic activity or readily undergo photocorrosion and/or inhibition. The search for a photocatalyst with all the positive features of titania as a photocatalyst and an ability to absorb visible as well as UV light is one of the continuing great quests in photochemistry.

3.4. *Photocatalyst activity: Effect of final annealing temperature*

Usually in the sol–gel synthesis of titania, the titania is largely in an amorphous, hydrated form, $Ti(OH)_4$, and the final high temperature annealing step

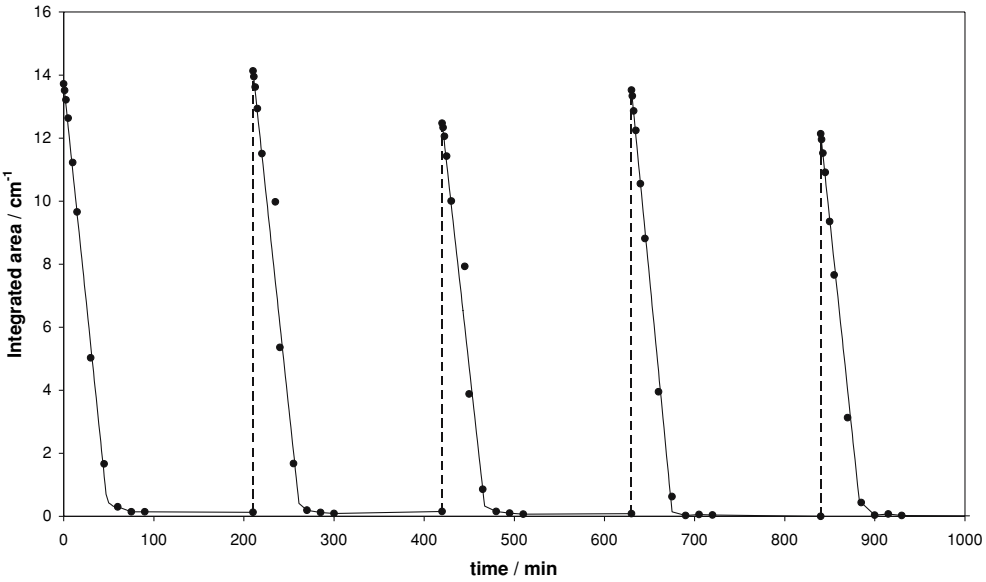

Fig. 5. Plot of a profile of the integrated area under the stearic acid peaks as a function of irradiation time, recorded using the same thick TiO_2 paste film. The broken lines indicate the point of addition of a further amount of stearic acid after the complete removal of the previous one [8].

($T \geq 450$ °C) promotes the processes of dehydration and crystallisation, often leading to the formation of anatase particles [16–18]. However, the hydro-thermal particle growth step employed here in the preparation of the titania thick paste appears not only to promote particle growth, but also crystallisation. Thus, XRD analysis of the final paste reveals the titania particles to be largely anatase even before the final heat-treatment step is applied. Although the photocatalytic activities of an annealed (450 °C for 30 min) and non-annealed thick titania paste film are the very similar, at higher annealing temperatures the photocatalytic activity of the film is expected to change, either due to particle sintering or a change in crystal phase (from anatase to rutile). In a study of this effect, the photocatalytic activities of the thick paste films were measured, as a function of final annealing temperature, applied for 30 min to a set of typical non-annealed films. In this work quartz was used as the glass substrate in order to allow the application of high (up to 900 °C) annealing temperatures and each film generated was also characterised by UV/Vis spectrophotometry, XRD, AFM and profilometry.

The measured variation in UV/Vis spectrum of these films as a function of annealing temperature is illustrated in Figure 6 and reveals that whereas there is little

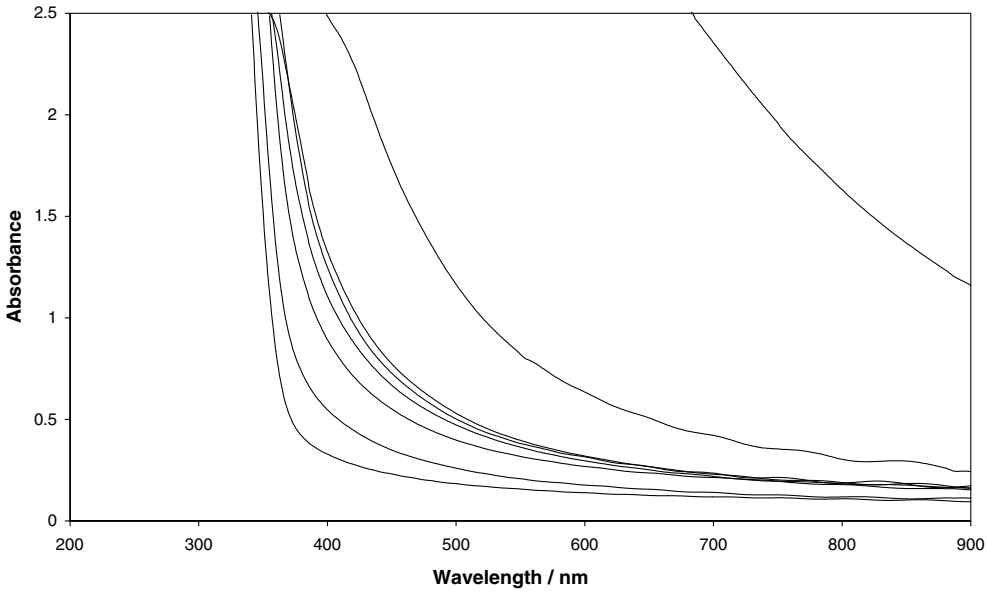

Fig. 6. UV/visible absorbance spectra for a series of thick paste films (initially, ca. 4.5 μm thick) annealed at the following temperatures for 30 min (from left to right): 450, 700, 730, 740, 750, 760, 800 and 900 °C, respectively.

difference between the absorption spectrum of a film annealed at 450 °C and one annealed at 700 °C, the films become more opalescent and light-scattering as the annealing temperatures is increased above 700 °C. In particular, the films become highly scattering at annealing temperatures > 760 °C, and, as a consequence, films annealed at 900 °C are white and opaque. This variation in UV/Vis absorption spectrum is mainly due to particle growth through sintering.

Direct evidence for the sintering of titania particles in the thick paste films, with annealing temperatures > 760 °C, was gained from an AFM study of the different films, some of the results of which are illustrated in Figure 7. Thus, although the AFM's of the 450 and 700 °C annealed films are quite similar, comprising particles typically 50–60 nm in diameter, films annealed at 800 °C and, especially, 900 °C are comprised of much bigger particles, i.e. typically, 99 and 217 nm, respectively. From this AFM study it is not surprising that the films become more scattering at high annealing temperatures, since particle growth is significant at these elevated temperatures, especially at temperatures ≥800 °C.

Particle growth at temperatures ≥ 800°C is important, but another critical process, which should not be ignored, is the phase change of titania from anatase to rutile, which also occurs in this region and a good way to study this process is through the use of XRD. Thus, the variation in the XRDs of the annealed titania films was studied as a function of annealing temperature and the results of this work are illustrated in Figure 8(a). Anatase titania has major XRD peaks associated with the following crystal planes and spacings, i.e. (*hkl*, *d*/Å): (101, 3.51), (200, 1.89), (0 0 4, 2.38) and (05, 1.70), respectively, whereas rutile has peaks at: (110, 3.25), (211, 1.69), (101, 2.49) and (111, 2.19), respectively. Given that the wavelength of the X-radiation used in this work was 1.5406 Å, and the value of *d* is related to the Bragg angle associated with a specific crystal spacing, θ, via the following equation:

$$d(\text{in Å}) = 1.5406/(2\sin\theta) \tag{5}$$

It follows that anatase is expected to exhibit major peaks at 2θ values of: 25.4°, 48.1°, 37.8° and 53.9° and rutile at: 27.4°, 54.3°, 36.1° and 41.2 ° and some, or all,

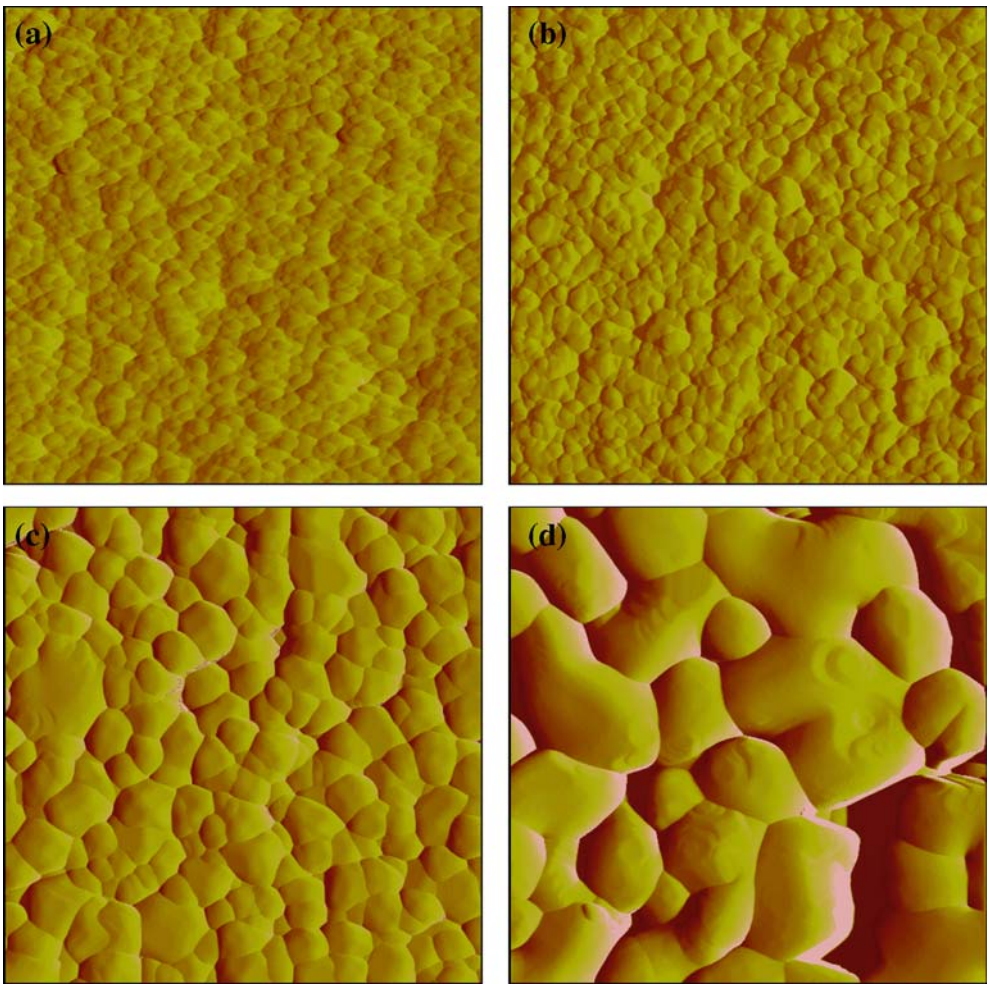

Fig. 7. AFM images of a series of thick paste films (initially, ca. 4.5 μm thick) annealed at the following temperatures for 30 min: (a) 450, (b) 700, (c) 800 and (d) 900 °C, respectively; all illustrated AFM's are for a scanned area of 1 μm^2.

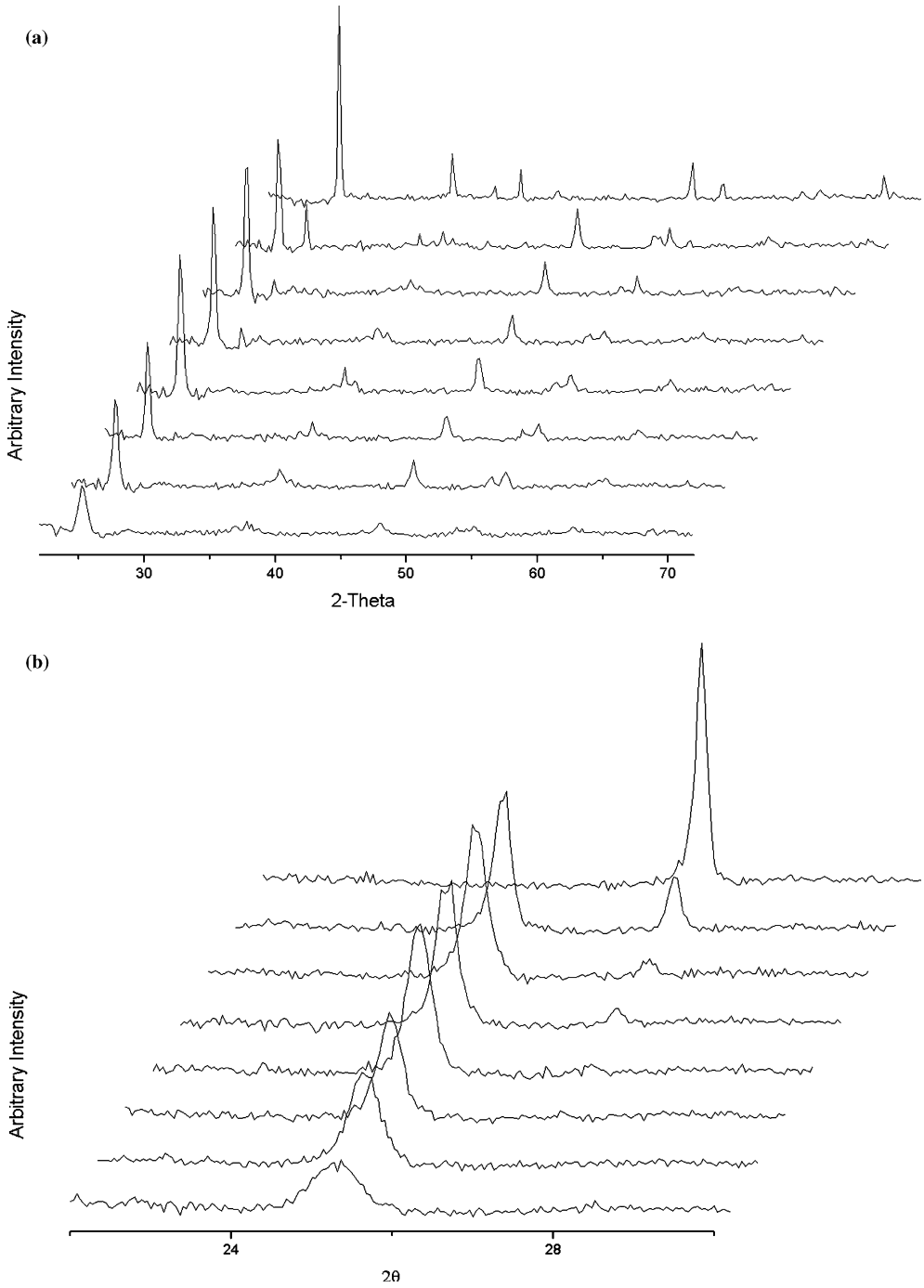

Fig. 8. (a) Powder XRD patterns recorded for a series of thick paste films (initially, ca. 4.5 μm thick) annealed at the following temperatures for 30 min (front to back): 450, 700, 730, 740, 750, 760, 800 and 900 °C, respectively. (b) Enlargement of the XRD spectra in (a), spanning the range $22 \leq 2\theta \leq 30$.

of these peaks can be seen in the XRD spectra illustrated in figure 8(a). Figure 8(b) illustrates an expanded section in the XRD spectra in Figure 8(a) and shows that with increasing annealing temperature, the presence of rutile (major peak (110) at $2\theta = 27.4°$) in the film emerges only at annealing temperatures ≥ 740 °C and in significant amounts only $T \geq 800$ °C. In addition, in all films annealed at temperatures < 900 °C, anatase is the predominant species. Spurr and Meyers used the intensities of the lines at $2\theta = 25.4°$ for the (101) plane of anatase and $2\theta = 27.4°$ for the (110) plane of rutile, i.e. the lines depicted in figure 8(b), to calculate the fraction of anatase, x_A, using the following expression:

$$x_A = \frac{1}{1 + 1.26(I_R/I_A)} \tag{6}$$

where I_R and I_A are the intensities of the reflections for the (110) plane of rutile and the (101) plane of anatase, respectively [19]. Using this formula, and the data in figure 8(b), the variation in x_A was determined as a function of annealing temperature and the results of this

work are illustrated in figure 9. The results show that the level of rutile in the films is only ca. 25% even at an annealing temperature of 800 °C and that only at 900 °C is the film fully transformed in rutile.

From the peak width of the XRD peaks at $2\theta = 25.3$ and 27.4 it is possible to estimate the average size of the crystal domains in each of the films as a function of annealing temperature using the Scherrer equation [20]. A plot of particle size, as measured by AFM, versus crystal domain size, as calculated from XRD data using the Scherrer equation, is illustrated in figure 10 and shows that at low annealing temperatures, i.e. ≤ 730 °C, the particle size is almost independent of annealing temperature, whereas the crystal domain size increases markedly. Thus, at these low annealing temperatures, crystal growth within particles dominates over the process of particle sintering and growth. At higher annealing temperatures, i.e. ≥ 740 °C, particle growth is more significant than crystal growth, with the size of the titania particles growing due to particle sintering ca. 5–6 times faster than that of crystal domain size.

Of critical significance to a self-cleaning film is the observed variation in its photocatalytic activity as a function of annealing temperature. In this work the measured rates of destruction of stearic acid, via Reaction (3) for each of the annealed films was used to assess the variation in the photocatalytic activity of the thick paste TiO_2 films as a function of annealing temperature and the results of this work are illustrated in Figure 11.

The significant feature of these results is the marked loss of photocatalytic activity of the titania films annealed at temperatures ≥ 760 °C. This loss as a function of annealing temperature does not correspond very well, with either the observed variation in particle or crystal domain size, or with the crystal phase, with annealing temperature. Thus, at 760 °C the particle size and crystal domain sizes are still relatively small (i.e. 82 and 24 nm, respectively) and there is little rutile present (7%). Instead, the drop in photocatalytic activity, illustrated in Figure 11, appears to correlate best with the apparent change in the porosity of the film. An approximate estimate of the fractional porosity, p, of the film can be made using the following formula:

$$p = \frac{h - h_0}{h} \tag{7}$$

where h and h_0 are the thicknesses of paste titania films with porosities, p, and zero, respectively.

In this work the thicknesses of all the films were measured by profilometry. Assuming that the films annealed at 900 °C have zero porosity, (AFM analysis of these films show them to be very compact), then the measured value of its thickness, which is 2.13 μm, is, according to Equation (7), h_o. Using this value for h_o, and the measured thicknesses for the other films and Equation (7), it is possible to calculate the variation in porosity, p, as a function of film annealing temperature and these results are illustrated in Figure 12. Some support for this approach for estimating porosity is that the value calculated using Equation (7), 51%, for 450 °C annealed films, is similar to that estimated for similar films by others [21], using gas adsorption methods (50–60%). Significantly, a plot of film photocatalyst rate versus its calculated porosity yields a good straight line, as illustrated by the insert diagram in Figure 12, i.e. there appears to be a linear correlation between the photocatalytic activity of a titania film and its porosity.

As noted earlier, the apparently low photocatalytic activity of commercial self-cleaning titania films, made by CVD, has been attributed previously to the low porosity of these materials, compared to most sol–gel

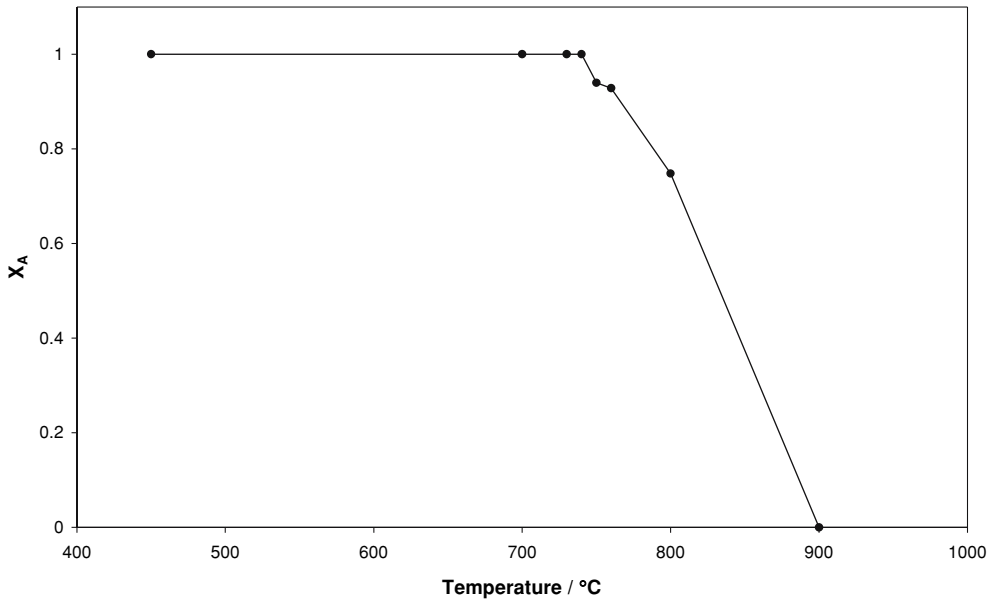

Fig. 9. Fraction of particles that are in the anatase form, x_A, as a function of film annealing temperature. The values of x_A for the different films were calculated using Equation (6) and the intensity data in Figure 8.

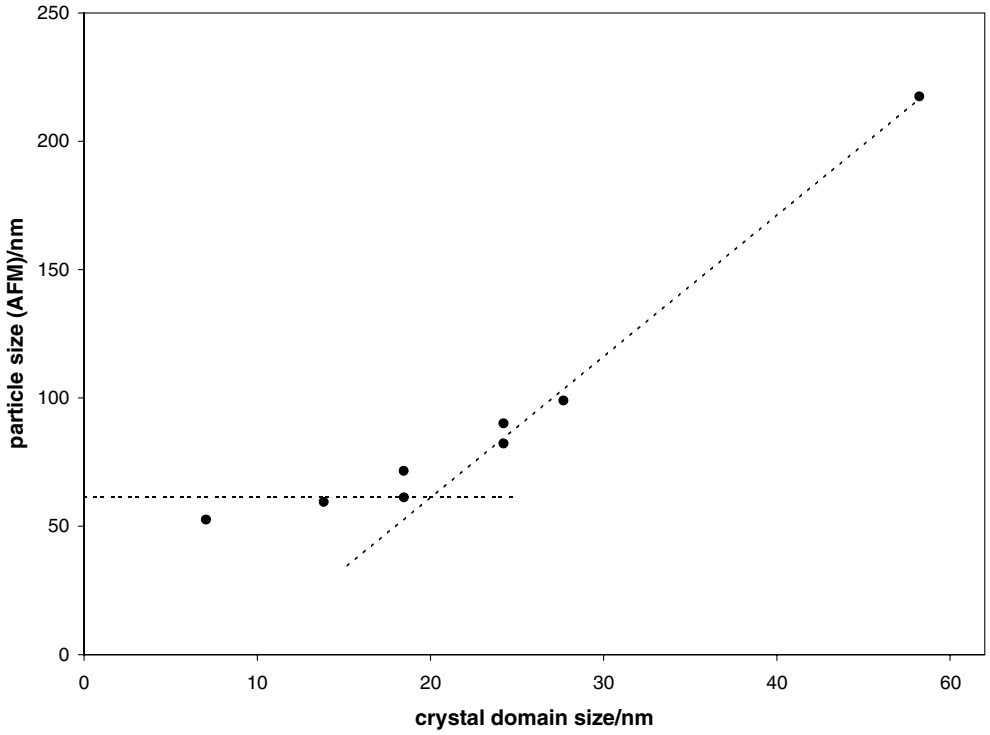

Fig. 10. Plot of particle size, as measured by AFM and crystal domain size, as measured using the data in Figure 8 and the Scherrer equation [20], for the different thick paste TiO_2 films annealed at different temperatures.

films [8]. One possible way in which porosity might be expected to positively influence photocatalyst activity is by providing a route, other than through the largely gas-impermeable stearic acid layer, for oxygen to diffuse to the active sites; effectively a 'fire-grate' effect. The prolonged photocatalytic mineralisation of organics by semiconductor photocatalysis is not possible without oxygen; the overall process is, after all, simply the photocatalysed 'cold-combustion' of the organic material. A porous film might be expected to provide channels through which the essential co-reactant, oxygen can diffuse to the surfaces of the titania and allow the photocatalytic process to occur unhindered. In contrast, a compact, non-porous, titania film will lack such channels, the rate of diffusion to the active sites will be expected to be less and, as a consequence, the rate of overall photocatalysis will be slower.

In a fire-grate, the rate of combustion can be controlled to some extent by the position of the grate. When open, the access of air to the burning embers

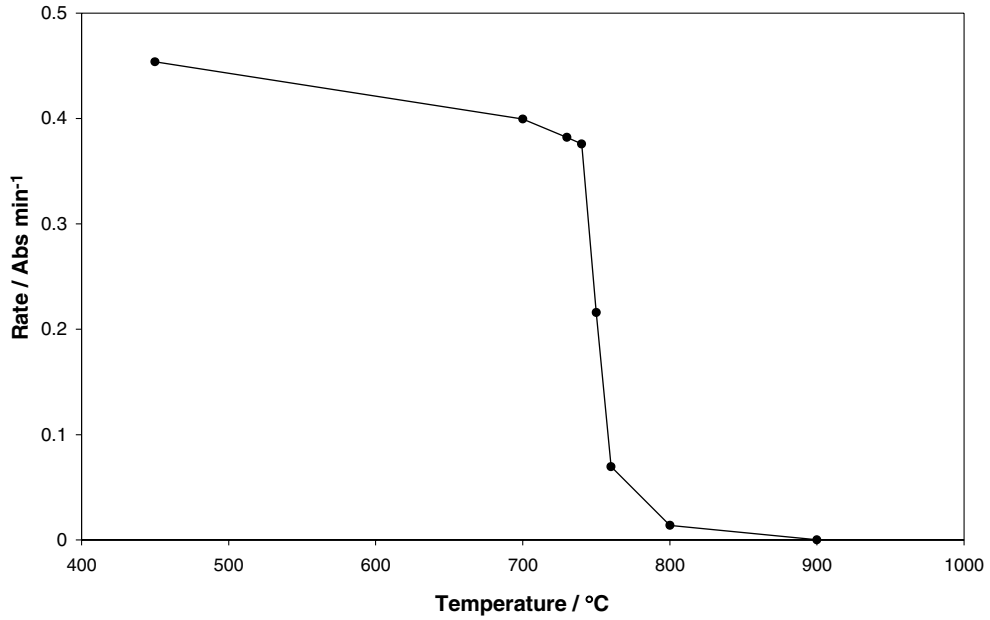

Fig. 11. Measured initial rate of the photocatalytic destruction of stearic acid as a function of annealing temperature for the thick paste TiO_2 films.

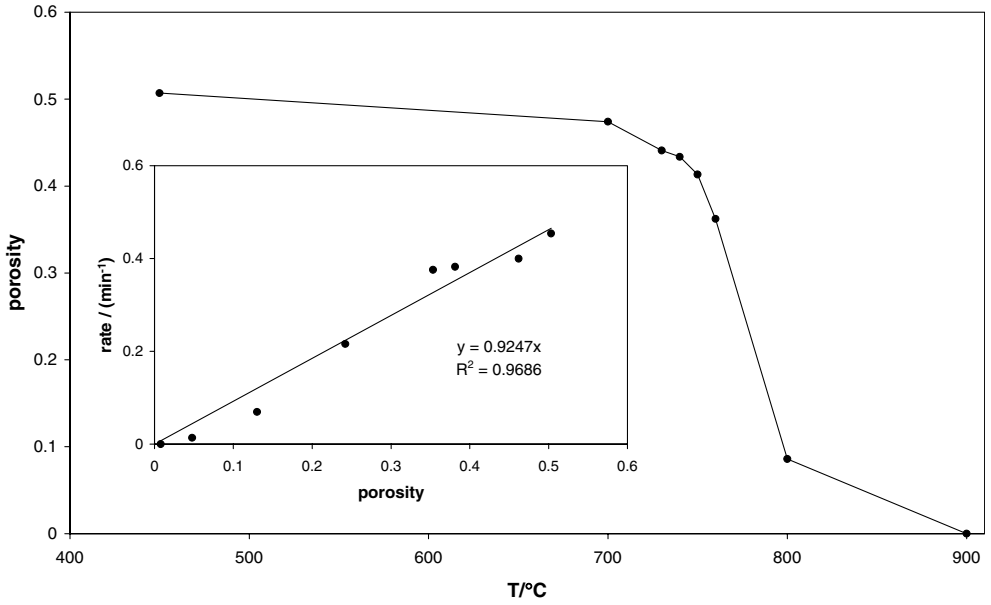

Fig. 12. Calculated variation in the porosity of the thick paste films, determined using Equation (7) and film thickness data obtained by profilometry, as a function of film annealing temperature. The insert diagram highlights the apparent linear relationship between the measured rate of photocatalysis (data from Figure 11) and the calculated porosity (from main diagram) for the thick paste TiO_2 films annealed at different temperatures.

nearest the grate is unlimited and combustion is rapid. When closed, the flow of air is appreciably curtailed and combustion is greatly reduced. As a consequence, the enhanced photocatalytic activity of porous titania films may be likened to an 'open fire-grate' effect, whereas the markedly reduced activity of compact, non-porous films is like a 'closed fire-grate' effect.

Although, from the results of this work, film porosity appears to be an important, and until now largely unrecognised, parameter in deciding the overall photocatalytic activity of titania films, the role of crystal phase may be just as important and should not be ignored. Certainly some researchers report rutile to be inactive as a photocatalyst material [22, 23], whereas others, after taking into consideration its usually reduced specific surface area, have found it to be similar in activity as anatase [24, 25]. In order to separate the roles of crystal phase and porosity on photocatalytic activity more work is required. In particular the generation of thick paste, porous rutile films of similar particle sizes and morphology to the ones reported in this work and thin, non-porous rutile and anatase films would help resolve some of these issues. Further work is in progress to develop such materials.

4. Conclusions

Thick paste TiO_2 films are optically clear, durable and very active as photocatalysts for the destruction of stearic acid on their surfaces. Although all the key features of such photocatalyst films are unchanged at annealing temperatures below 700 °C, above this temperature they are altered markedly. Thus, the films become increasing opaque, especially at temperatures >760 °C and much less active. The marked decrease in photocatalytic activity appears to correlate well with the change in the calculated porosity of thick paste films as a function of annealing temperature. This finding may help explain the low photocatalytic activity associated with most commercial samples of self-cleaning glass, since their active outer coating usually comprises nancrystalline, non-porous thin films of titania.

References

1. R. Bridgeman, *1000 Inventions and Discoveries* (Dorling, Kindersley, 2002).
2. V. Ashton, *Chem. Brit*. June (2002) 26.
3. A. Mills and S. LeHunte, *J. Photochem. Photobiol. A: Chem*. **108** (1997) 1.
4. A. Fujishima, T.N. Rao and D. Tryk, *J. Photochem. Photobiol. C: Photochem. Rev*. **1** (2000) 1.
5. A. Mills and S.-K. Lee, *J. Photochem. Photobiol. A: Chem*. **152** (2002) 233.
6. A. Mills, A. Lepre, N. Elliott, S. Bhopal, I.P. Parkin and S.A. O'Neill, *J. Photochem. Photobiol. A: Chem*. **160** (2003) 213.
7. A. Mills, S.-K Lee, A. Lepre, I.P. Parkin and S.A. O'Neill, *Photochem. Photobiol. Sci*. **1** (2002) 865.
8. A. Mills, G. Hill, S. Bhopal, I.P. Parkin and S.A. O'Neill, *J. Photochem. Photobiol. A: Chem*. **160** (2003) 185.
9. A. Mills, N. Elliott, G. Hill, D. Fallis, J.R. Durrent and R.L. Willis, *Photochem. Photobiol. Sci*. **2** (2003) 591.
10. S.-K. Lee, S. McIntyre and A. Mills, *J. Photochem. Photobiol. A: Chem*. **162** (2004) 203.
11. Y. Paz, Z. Luo, L. Rabenberg and A. Heller, *J. Mater. Res*. **10** (1995) 2842.
12. A. Zaban, S.T. Aruna, S. Tirosh, B.A. Gregg and Y. Mastai, *J. Phys. Chem. B* **104** (2002) 4130.
13. P. Sawanyama, L. Jiang, A. Fujishima and K. Hashimoto, *J. Phys. Chem. B* **101** (1997) 11000.

14. T. Minabe, D.A. Tryk, P. Sawanyama, Y. Kikuchi, K. Hashimoto and A. Fujishima, *J. Photochem. Photobiol. A: Chem.* **137** (2000) 53.
15. S. Sitkiewitz and A. Heller, *New J. Chem.* **20** (1996) 233.
16. S. Doeff, M. Henry, C. Sanchez and J. Livage, *J. Non-Cryst. Solids* **89** (1987) 206.
17. J. Livage and C. Sanchez, *J. Non-Cryst. Solids* **145** (1992) 11.
18. F. Babonneau, C. Sanchez and J. Livage, *J. Non-Cryst. Solids* **106** (1988) 170.
19. R.A. Spurr and H. Myers, *Anal. Chem.* **29** (1957) 760.
20. H.P. Klug and L.E. Alexander, *X-Ray Diffraction Procedures for Polycrystalline and Amorphous Materials* (Wiley, NY, 1954), p. 512.
21. C.J. Barbé, F. Arendse, P. Comte, M. Jirousek, F. Lenzmann, V. Shklover and M. Grätzel, *J. Am. Ceram. Soc.* **80** (1997) 3157.
22. K. Okamoto, Y. Yamamoto, H. Tanaka and A. Itaya, *Bull. Chem. Soc. Jpn.* **58** (1985) 2015.
23. V. Augugliaro, L. Palmisano, A. Sclafani, C. Minero and E. Pelizzetti, *Toxicol. Environ. Chem.* **16** (1988) 89.
24. A. Sclafani, L. Palmisano and M. Schiavello, *J. Phys. Chem.* **94** (1990) 829.
25. A. Mills and S. Morris, *J. Photochem. Photobiol. A: Chem.* **71** (1993) 285–289.